Analysis and control of the dynamical response of a higher order drifting oscillator

Yang Liu[a], Joseph Páez Chávez[b,d], Ekaterina Pavlovskaia[c], Marian Wiercigroch[c]

[a] *College of Engineering Mathematics and Physical Sciences, University of Exeter, Rennes Drive, Exeter EX4 4RN, UK*
[b] *Center for Applied Dynamical Systems and Computational Methods (CADSCOM), Faculty of Natural Sciences and Mathematics, Escuela Superior Politécnica del Litoral, P.O. Box 09-01-5863, Guayaquil, Ecuador*
[c] *Centre for Applied Dynamics Research, School of Engineering, University of Aberdeen, Aberdeen AB24 3UE, UK*
[d] *Center for Dynamics, Department of Mathematics, TU Dresden, D-01062 Dresden, Germany*

Abstract

This paper studies a position feedback control strategy for controlling a higher order drifting oscillator which could be used in modelling of the vibro-impact drilling. Special attention is given to two control issues, eliminating bistability and suppressing chaos, which may cause inefficient and unstable drilling. Numerical continuation methods implemented via the continuation platform COCO are adopted to investigate the dynamical response of the system. Our analyses show that, the proposed controller is capable of eliminating coexisting attractors and mitigating chaotic behaviour of the system, providing that its feedback control gain is chosen properly. Our investigations also reveal that, when the slider's property modelling the drilled formation changes, the rate of penetration for the controlled drilling can be significantly improved.

Keywords: Vibro-impact drilling, position feedback control, progression optimization, bistability, chaos control

1. Introduction

The adoption of the vibro-impact principle for drilling tools, known as downhole hammer, percussive hammer, or percussive drills [1], has been used for construction, and later for oil and gas exploration since the late 1940s. The operating principle of such technique is that, penetration can be achieved by repeatedly applying a large impulsive force to the drill-bit through a hydraulically or pneumatically operated piston impacting axially upon a drilling rod, and transferring the potential energy into kinetic energy of the drill-bit [2]. The merit of this mechanism is that rocks can be chipped and crushed easily by the impulsive force from the drill-bit, so that the rate of penetration (ROP) of the entire drill-string can be enhanced. Normally, the vibro-impact drilling can significantly reduce wellbore creation time, and it is especially suitable for hard rocks [3]. In order to improve the performance of this technique, various drifting oscillator models [4–10], which can effectively predict overall dynamics and progressive motion of the vibro-impact drilling, have been studied in the past two decades. The main aim of these studies is to fully understand the dynamics of the drifting oscillators under various control parameters and optimize its ROP. In [4], Pavlovskaia et al. studied the physical model of an impact system with a drift which can represent a number of practical driving tools, and revealed that the fastest penetration occurs when the system responds periodically. In [11], a simple control strategy was considered for this drifting system to improve its progression rates. This study suggests that, the work which is done by the control forces must be positive in order to supply additional external energy to the system. In [5], an efficient semi-analytical method was developed for the drifting system to predict a range of control parameters for which the best progression rates were achieved. Luo et al. [6] studied a two-degree-of-freedom plastic impact oscillator with a frictional slider, and the largest progression was observed when

Email addresses: y.liu2@exeter.ac.uk (Yang Liu), jpaez@espol.edu.ec (Joseph Páez Chávez), e.pavlovskaia@abdn.ac.uk (Ekaterina Pavlovskaia), m.wiercigroch@abdn.ac.uk (Marian Wiercigroch)

period-1 single-impact sticking motion with large impact velocity occurred. In [7], a vibro-impact moling rig, which was based on electro-mechanical interactions of a conductor with an oscillating magnetic field, was studied numerically and experimentally. Recently, modelling of the high frequency vibro-impact drilling was undertaken in [12]. In this study, a newly developed model of an existing experimental rig [3] was compared with the simplified low dimensional model [4] which was created to describe the dynamic interaction between the drill-bit and the drilled formation. The best progression rates were identified through bifurcation analysis and they were observed when the system response was periodic and the frequency of the response was the same as the frequency of the applied dynamic force. Until now, few works (e.g. [13]) have considered optimization of the vibro-impact drilling from a feedback control point of view, i.e. the question on how to best utilise system information as feedback signal to improve the ROP and the stability of vibro-impact drilling still remains open. This question defines the rationale of this paper, which considers utilising the displacement of the drill-bit as feedback to modulate the impulsive forces, and gives insight into its controlled dynamics for drilled rock formations.

Control of vibro-impact systems has been a great interest of scientific research, e.g. [14–18], and the main concern of these studies has been on how to suppress chaotic motion and maintain the stability of the system under the noise present environment. In general, two non-smooth nonlinearities, namely impact and friction, are involved in these vibro-impact systems, which lead to their complexities in dynamics and sensitivities to external disturbances. Therefore, control strategy must be in place to ensure their stabilities, particularly for their rich dynamical phenomena at near-grazing dynamics [19, 20]. In [14], de Souza and Caldas proposed a new procedure to implement the OGY method to control the chaotic orbits in mechanical system with impacts. Dankowicz and Jerrelind [15] studied a linear, discrete, and closed-loop control strategy for ensuring the persistence of a local attractor in the near-grazing dynamics of an impact oscillator. In [16], a feedback control technique was applied to suppress chaotic behaviour in dissipative mechanical systems by using a small-amplitude damping signal. Later on, this technique was considered to control the chaotic motions of a number of vibro-impact and non-ideal oscillators [17]. Suppressing bifurcation and chaotic-impact motions of a plastic impact oscillator was studied by Luo and Lv [18] by using an external driving force, delay feedback and damping control law.

Apart from controlling chaos in vibro-impact systems, Liu et al. [21] studied the switching control between coexisting attractors for multistable vibro-impact systems. This was carried out by bringing the perturbed state of the system into the basin of attraction of a desired attractor using a short impulsive force [22]. The switching control ensures low power consumption of the system [23, 24] while maintains the system at some level of flexibility since its multistability is not affected. On the other hand, redundant coexisting periodic orbits must be suppressed if they could induce undesired performance or instability to the system, which means the switching control is invalid here and the multistable vibro-impact system needs to be converted into a monostable system. For example, a vibro-impact capsule system with forward and backward drifts presents multistability when the contact between the capsule and its supporting surface is sticky [25]. Here, the multistability of the capsule is manifested through a number of periodic orbits with low progression rates and a chaotic motion. So, a position feedback controller was designed to control the capsule to a monostable system with the desired direction of progression (i.e. forward or backward) [26, 27]. In [8, 28], coexisting attractors have been found for the drifting oscillator, and it was observed that multistability may affect the performance of vibro-impact drilling. Therefore, in this paper, we will investigate this phenomenon further and study its influence on the ROP of vibro-impact drilling.

The rest of the paper is organized as follows. In Section 2, the physical model and equations of motion of the higher order drifting oscillator are introduced, as well as the mathematical formulation of the position feedback control law. In Section 3, the proposed control method is studied numerically, and its capabilities in eliminating bistability, mitigating chaos, and improving the ROP for different drilled formations are demonstrated through bifurcation analysis. Numerical investigation using the continuation methods, including one- and two-parameter analyses, is presented in Section 4. Finally, some concluding remarks are drawn in Section 5.

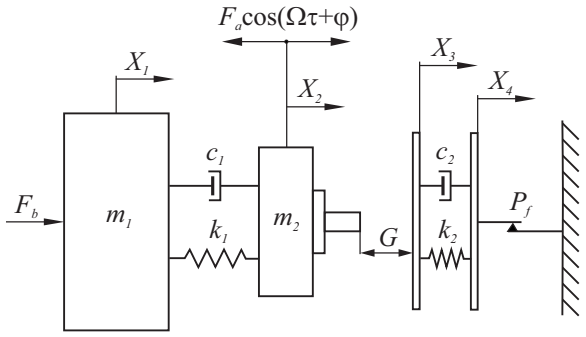

Figure 2.1: Physical model of the higher order drifting oscillator.

2. Mathematical modeling

The vibro-impact drilling model considered in this investigation is shown in Fig. 2.1, which corresponds to a higher order drifting oscillator with four degrees of freedom featuring soft impacts. The model includes a mass m_2 representing the drill-bit assembly, which is driven by an external sinusoidal force with amplitude F_a and frequency Ω. This mass interacts with another element (mass m_1) that accounts for all the components above the drill-bit assembly. A static force F_b is applied on m_1, and the interaction between m_1 and m_2 is represented via a linear spring with stiffness k_1 and a viscous damper with damping coefficient c_1. The interaction between the drill-bit and the rock formation is modeled by a frictional, massless visco-elastic slider with stiffness and damping coefficients k_2 and c_2, respectively. The slider moves right in stick-slip phases, with the progression taking place when the force acting on the slider becomes larger than the threshold of the dry friction force P_f. The variables X_1, X_2, X_3, and X_4 stand for the absolute position of the mass m_1, drill-bit assembly m_2, left slider plate and right slider plate, respectively. During operation, the condition $X_2 - X_3 \geq G$ is monitored, which is satisfied when the drill-bit assembly is in contact with the left plate of the frictional slider. Here, $G > 0$ represents an initial gap between the drill-bit and the frictional slider.

The higher order drifting oscillator shown in Fig. 2.1 is a simplified version of the vibro-impact drilling system studied in [12]. In the present work, we group all the components above the drill-bit into a single mass (m_1 in Fig. 2.1) in order to obtain a reduced form of the system considered in [12]. On the other hand, compared to the models studied in [4, 29], there is an extra degree-of-freedom, due to the presence of the mass m_1. The motivation for this is that the extra degree-of-freedom will allow us to understand the dynamics of the drill-bit under the constraint of other drill-string components, which provides a more realistic scenario in comparison with previous drifting oscillators of low dimension studied in the literature. In addition, the extra stiffness k_1 introduces the possibility of studying in more detail the physical properties of the drilled media represented by the visco-elastic slider shown in Fig. 2.1, by varying the ratio between k_1 and k_2, which has not been investigated in the literature before.

2.1. Equations of motion

According to the mechanical setup described previously, the higher order drifting oscillator can operate under any of the following regimes: *no contact*, *contact without progression*, and *contact with progression*. The operation mode *no contact* occurs when $X_2 - X_3 < G$, i.e., the drill-bit and the rock formation are not in contact. In this case, the motion of the system is governed by the set of equations

$$\begin{cases} m_1\ddot{X}_1 + c_1(\dot{X}_1 - \dot{X}_2) + k_1(X_1 - X_2) = F_b, \\ m_2\ddot{X}_2 + c_1(\dot{X}_2 - \dot{X}_1) + k_1(X_2 - X_1) = F_a\cos(\Omega\tau + \varphi) + U_p, \\ c_2(\dot{X}_3 - \dot{X}_4) + k_2(X_3 - X_4) = 0, \\ \dot{X}_4 = 0, \end{cases} \tag{2.1}$$

where

$$U_p = K_p(X_4 - X_2), \tag{2.2}$$

is a position controller with control gain K_p. This operation mode terminates when the mass m_2 hits the left plate of the frictional slider (see Fig. 2.1), which occurs precisely when $X_2 - X_3 = G$. After this, the system switches to one of the contact modes, *contact without progression* or *contact with progression*, depending on the force acting on the slider at the moment of contact. If this force does not exceed the dry friction threshold P_f, the system switches to *contact without progression*, described by the system of ODEs

$$\begin{cases} m_1\ddot{X}_1 + c_1(\dot{X}_1 - \dot{X}_2) + k_1(X_1 - X_2) = F_b, \\ m_2\ddot{X}_2 + c_1(\dot{X}_2 - \dot{X}_1) + k_1(X_2 - X_1) + c_2(\dot{X}_3 - \dot{X}_4) + k_2(X_3 - X_4) = F_a\cos(\Omega\tau + \varphi) + U_p, \\ X_3 = X_2 - G,\ \dot{X}_3 = \dot{X}_2, \\ \dot{X}_4 = 0. \end{cases} \tag{2.3}$$

If the slider and the drill-bit are in contact, and the force acting on m_2 from the slider becomes larger than the dry friction threshold P_f, the system operates under the regime *contact with progression*, whose dynamics is governed by the equations

$$\begin{cases} m_1\ddot{X}_1 + c_1(\dot{X}_1 - \dot{X}_2) + k_1(X_1 - X_2) = F_b, \\ m_2\ddot{X}_2 + c_1(\dot{X}_2 - \dot{X}_1) + k_1(X_2 - X_1) + P_f = F_a\cos(\Omega\tau + \varphi) + U_p, \\ X_3 = X_2 - G,\ \dot{X}_3 = \dot{X}_2, \\ c_2(\dot{X}_3 - \dot{X}_4) + k_2(X_3 - X_4) = P_f. \end{cases} \tag{2.4}$$

2.2. Nondimensionalization and variable transformation

In our investigation, we will use the following dimensionless variables and parameters:

$$\begin{aligned} &\Omega_0 = \sqrt{\frac{k_2}{m_2}}, \quad \omega = \frac{\Omega}{\Omega_0}, \quad t = \Omega_0\tau, \quad a = \frac{F_a}{P_f}, \quad b = \frac{F_b}{P_f}, \quad \zeta = \frac{c_2}{2m_2\Omega_0}, \\ &g = \frac{k_2}{P_f}G, \quad \alpha = \frac{m_2}{m_1}, \quad \beta = \frac{k_1}{k_2}, \quad \gamma = \frac{c_1}{c_2}, \quad x_1 = \frac{k_2}{P_f}X_1, \quad x_2 = \frac{k_2}{P_f}X_2, \\ &x_3 = \frac{k_2}{P_f}X_3, \quad x_4 = \frac{k_2}{P_f}X_4, \quad y_1 = \frac{\mathrm{d}x_1}{\mathrm{d}t}, \quad y_2 = \frac{\mathrm{d}x_2}{\mathrm{d}t}, \quad k_p = \frac{K_p}{k_2}\ . \end{aligned} \tag{2.5}$$

For numerical purposes, it is convenient to analyse the drifting oscillator as a piecewise-smooth dynamical system, which is a mathematical framework suitable for the application of path-following methods via the continuation platform COCO. Let us denote by $u := (z_1, w_1, z_2, w_2, z_3)^T \in \mathbb{R}^5$ and $\lambda := (\alpha, b, \beta, \gamma, \zeta, a, \omega, k_p, g, \varphi) \in \mathbb{R}^9 \times [0, 2\pi)$ the state variables and parameters of the piecewise-smooth system, respectively. The state variables defined here are related to those introduced in (2.5) via the linear transformation

$$\begin{cases} z_1 = x_1 - x_4, \\ w_1 = y_1, \\ z_2 = x_2 - x_4, \\ w_2 = y_2, \\ z_3 = x_3 - x_4, \end{cases} \tag{2.6}$$

which allows us to decouple the periodic behaviour of the system from the progression, as e.g. in [30]. In this setting, the vector fields to be used for the numerical implementation, after the transformations (2.5) and (2.6), are given by (one for each operation mode, see Section 2.1):

No contact (see Eq. (2.1)):

$$u' = f_{\text{NC}}(u,\lambda,t) := \begin{pmatrix} w_1 \\ \alpha b - \alpha\beta(z_1 - z_2) - 2\alpha\gamma\zeta(w_1 - w_2) \\ w_2 \\ \beta(z_1 - z_2) + 2\gamma\zeta(w_1 - w_2) + \left[a\cos(\omega t + \varphi) - k_p z_2\right] \\ -\dfrac{1}{2\zeta} z_3 \end{pmatrix}, \tag{2.7}$$

where the prime denotes the derivative with respect to the non-dimensional time t.
Contact without progression (see Eq. (2.3)):

$$u' = f_{\text{C1}}(u,\lambda,t) := \begin{pmatrix} w_1 \\ \alpha b - \alpha\beta(z_1 - z_2) - 2\alpha\gamma\zeta(w_1 - w_2) \\ w_2 \\ \beta(z_1 - z_2) + 2\gamma\zeta(w_1 - w_2) - 2\zeta w_2 - z_3 + \left[a\cos(\omega t + \varphi) - k_p z_2\right] \\ w_2 \end{pmatrix}. \tag{2.8}$$

Contact with progression (see Eq. (2.4)):

$$u' = f_{\text{C2}}(u,\lambda,t) := \begin{pmatrix} w_1 - w_2 - \dfrac{1}{2\zeta}(z_3 - 1) \\ \alpha b - \alpha\beta(z_1 - z_2) - 2\alpha\gamma\zeta(w_1 - w_2) \\ -\dfrac{1}{2\zeta}(z_3 - 1) \\ \beta(z_1 - z_2) + 2\gamma\zeta(w_1 - w_2) - 1 + \left[a\cos(\omega t + \varphi) - k_p z_2\right] \\ -\dfrac{1}{2\zeta}(z_3 - 1) \end{pmatrix}. \tag{2.9}$$

In this mathematical framework, the system can be written in compact form as follows

$$u' = \begin{cases} f_{\text{NC}}(u,\lambda,t), & h_{\text{IMP}}(u,\lambda) < 0 \ \text{ or } \ h_{\text{C1}}(u,\lambda) \le 0, \\ f_{\text{C1}}(u,\lambda,t), & h_{\text{IMP}}(u,\lambda) = 0 \ \text{ and } \ 0 < h_{\text{C1}}(u,\lambda) < 1, \\ f_{\text{C2}}(u,\lambda,t), & h_{\text{IMP}}(u,\lambda) = 0 \ \text{ and } \ h_{\text{C1}}(u,\lambda) \ge 1, \end{cases} \tag{2.10}$$

where

$$h_{\text{IMP}}(u,\lambda) := z_2 - z_3 - g \ \text{ and } \ h_{\text{C1}}(u,\lambda) := 2\zeta w_2 + z_3,$$

are event functions used to detect the transitions between the operation modes of the system.

Notice that the dimension of the model has been reduced by 1 (see Eq. (2.1), (2.3) and (2.4)). This is because the progression (captured by the variable x_4) of the system has been decoupled from the model. The progression, however, can be reconstructed from the system (2.10) as follows. Consider a solution $u(t) = (z_1(t), w_1(t), z_2(t), w_2(t), z_3(t))^T$ of (2.10), for $t \ge 0$. Then

$$x_4(t) = x_4^0 + \int_0^t v(\tau)\, d\tau,$$

where $x_4^0 \in \mathbb{R}$ represents an initial position at the beginning of current progression phase, and

$$v(t) = \begin{cases} w_2(t) + \dfrac{1}{2\zeta}(z_3(t) - 1), & h_{\text{IMP}}(u(t), \lambda) = 0 \ \text{ and } \ h_{\text{C1}}(u(t), \lambda) \geq 1, \\ 0, & \text{otherwise}, \end{cases}$$

which gives the velocity of the right plate of the slider for all $t \geq 0$ (see Eq. (2.1)–(2.6)). If, in addition, the solution $u(t)$, $t \geq 0$, is periodic with period $T_0 > 0$, the ROP can be computed as

$$\text{ROP} := \frac{1}{T_0}(x_4(T_0) - x_4^0),$$

which represents the average velocity of the right plate of the frictional slider shown in Fig. 2.1, during one period of motion.

3. Bifurcation Analysis

In the following subsections, we will analyze the behaviour of the higher order drifting oscillator via monitoring the velocity of the mass m_2, y_2 and calculating the ROP.

3.1. Controlling bistability

Bistability of the vibro-impact drilling has been observed by Pavlovskaia and Wiercigroch [30], Ajibose et al. [8], and Páez Chávez et al. [28], and it is clear that some of the coexisting attractors have higher progression rates than others. Fig. 3.1 presents a series of bifurcation diagrams which shows the main attractors of the vibro-impact drilling with large amplitude coexisting with the attractors (red dots) with small amplitude which have no penetration under variation of static force b. The inner windows on the left panels present the system trajectories on the phase plane (x_2-x_4, y_2), and the locations of the impact surface, which represent the contact of the drill-bit and the left plate of the frictional slider, are shown by blue lines. The inner windows on the right panels show the time histories of displacements of the drill-bit x_2 (black solid lines) and the slider bottom x_4 (red dash lines). As can be seen from Fig. 3.1(a), bistable attractors exist for $b \in [0.154, 0.208]$ and the best ROP is recorded at $b = 0.2$. This coexistence may cause the drilling inefficiency such that the state of the system hops from the main attractor with large amplitude to the one with small amplitude due to external perturbations. As the amplitude of excitation a increases, ROP increases and this bistability can be observed at the regimes where the best ROPs were recorded as shown in Fig. 3.1(b)-(d). In other words, there is always the risk that the vibro-impact drilling becomes inefficient when the system is operated at the regime of the best ROP. Compared with the ROP of the low order drifting oscillator studied in [4], where the best ROP was obtained when the static force was approximately 50% of the amplitude of excitation, our calculations show that the required static force is larger, more than 80% of the amplitude of excitation. This is due to the fact that, the extra degree-of-freedom, i.e. the components above the drill-bit assembly, causes reduced progression rates and the new optimum regime of the operating control parameters. It is also noted from [12] that, the optimum static force there is 40-50% of the dynamic amplitude, so including other degrees of freedom has significant influence on the dynamics of the vibro-impact drilling which could increase or decrease this ratio.

Fig. 3.2 shows the bifurcation diagrams when the position feedback controller was applied. It can be seen from Fig. 3.2(a) that, when $k_p = 0.03$, the regime of bistability has shrunk to $b \in [0.258, 0.272]$. As the control gain k_p increases, the coexisting attractors disappear in Fig. 3.2(b), and the system becomes monostable. However, the compromise is that the ROP of the drifting oscillator was reduced, and the best ROP was recorded at $b = 0.174$.

3.2. Suppressing chaos

It has been revealed in the literature (e.g. [4, 12]) that, insufficient static force b could lead to chaotic motion causing instability of the vibro-impact drilling. This has been shown in the left panels of Fig.

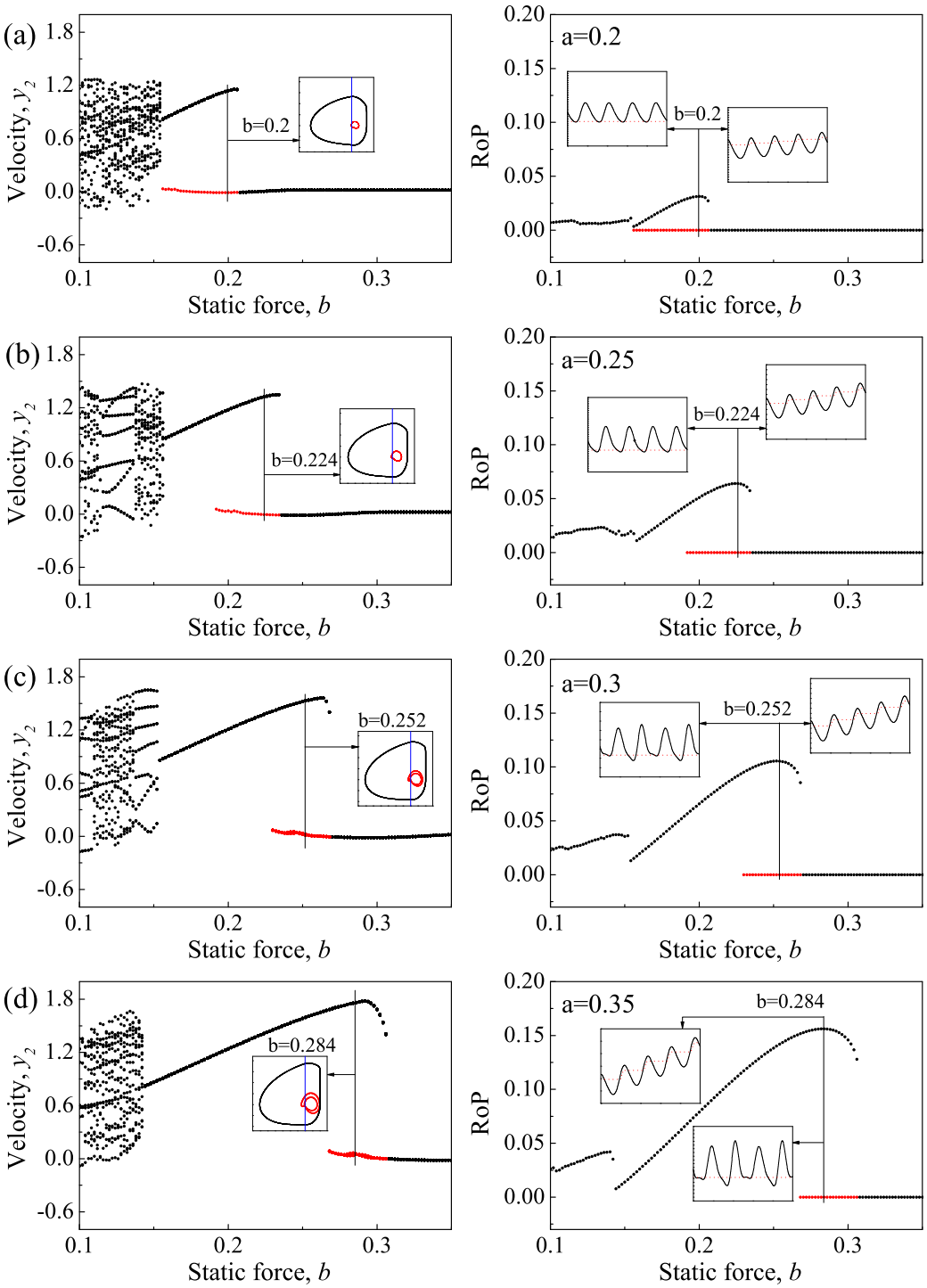

Figure 3.1: (Colour online) Bifurcation diagrams showing velocities (left panels) and ROPs (right panels) of the drifting oscillator calculated for $\alpha = 0.1$, $\beta = 0.1$, $\gamma = 1.0$, $\zeta = 0.05$, $g = 0.02$, $\omega = 0.53$, $\varphi = 0$, (a) $a = 0.2$, (b) $a = 0.25$, (c) $a = 0.3$, and (d) $a = 0.35$. Coexisting attractors are denoted by red dots in the bifurcation diagrams. The inner windows on the left panels present the system trajectories on the phase plane (x_2-x_4, y_2), and the locations of the impact surface are shown by blue lines. The inner windows on the right panels show the time histories of displacements of the drill-bit x_2 (black solid lines) and the slider bottom x_4 (red dash lines).

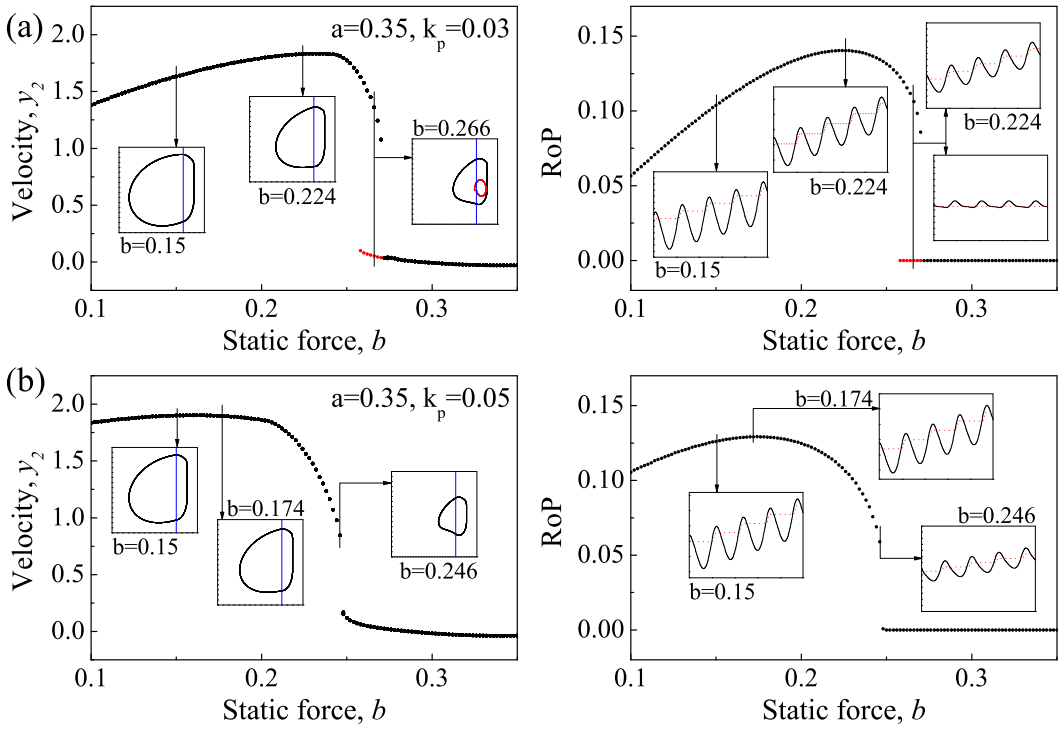

Figure 3.2: (Colour online) Bifurcation diagrams showing velocities (left panels) and ROPs (right panels) of the controlled drifting oscillator with (a) $k_p = 0.03$ and (b) $k_p = 0.05$ calculated for $\alpha = 0.1$, $\beta = 0.1$, $\gamma = 1.0$, $\zeta = 0.05$, $g = 0.02$, $\omega = 0.53$, $\varphi = 0$, $b = 0.2$, and $a = 0.35$. Coexisting attractors are denoted by red dots in the bifurcation diagrams. The inner windows on the left panels present the system trajectories on the phase plane (x_2-x_4, y_2), and the locations of the impact surface are shown by blue lines. The inner windows on the right panels show the time histories of displacements of the drill-bit x_2 (black solid lines) and the slider bottom x_4 (red dash lines).

3.3(a) and (b) under variation of excitation amplitude a, when $b = 0.1$ and $b = 0.15$, respectively. When the controller was applied, the chaotic motions were suppressed as demonstrated in the right panels of Fig. 3.3. ROPs before and after control at $b = 0.1$ and $b = 0.15$ were recorded in Fig. 3.4(a), which indicate the efficacy of the position feedback controller. This example demonstrate the effectiveness of the proposed controller on improving the ROP of vibro-impact drilling when static force is small. In order to show the dynamic behaviour of the system, Fig. 3.4(b) compares time histories of displacements of the drill-bit and the slider bottom for $a = 0.6$.

Another example is presented in Fig. 3.5, where chaotic motion (grey lines) was observed initially, and the system response became the period-1 motion with one impact per period of excitation after the control was applied at $t = 296.39$. It can be seen from Fig. 3.5(c) that, the control input u, where $u = a\cos(\omega t + \varphi) + u_p$, was increased significantly due to the input of the position feedback controller u_p. This can be interpreted as follows. When the control is not applied, large static force may help to maintain the periodic motion of the drill-bit, but this stability will be lost once static force becomes small. When the control is applied, it can preserve the stability of the drill-bit effectively. As can be seen from Eq. (2.2), when the distance between the drilled formation and the drill-bit $(x_4 - x_2)$ becomes large, the controller's input u_p is large and more energy will be injected into the drill-bit so that it can impact and crush the formation efficiently. Another observation can be found from the trajectory of the drill-string (green line) shown in Fig. 3.5(b), where harmful fluctuation of the drill-string was recorded initially, and it was stabilized when the control was applied.

3.3. Control of various slider properties

In practice, different formation properties may be encountered during drilling process, and optimal excitation depends on the properties of the formation/slider [31]. So, it is desirable to have the control

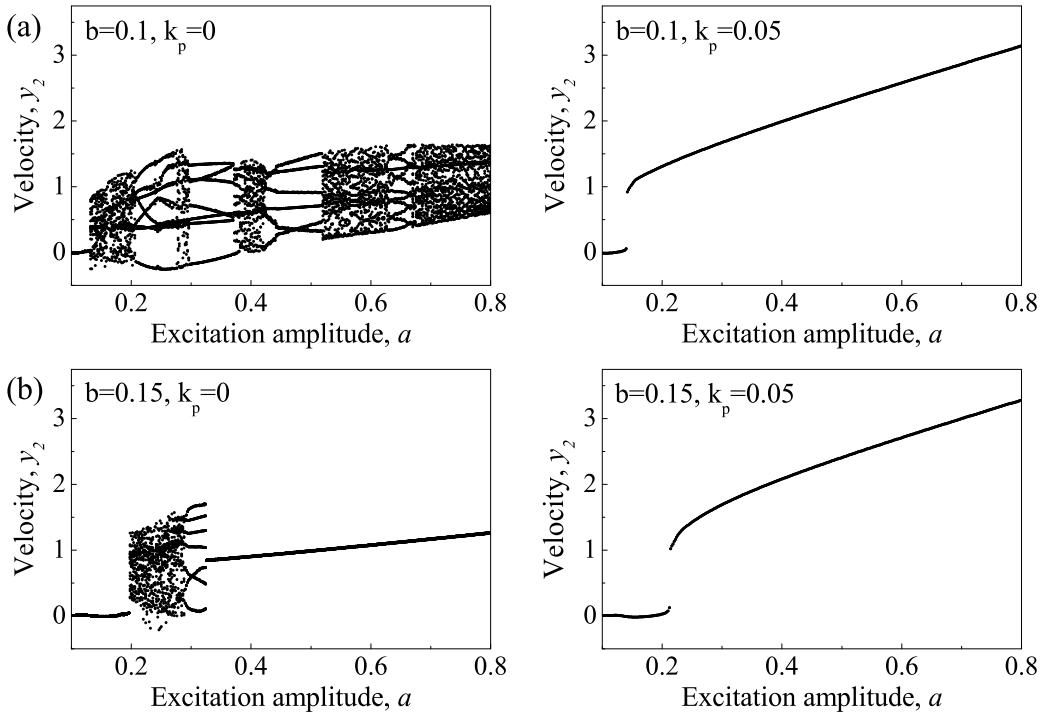

Figure 3.3: Bifurcation diagrams of the uncontrolled (left panels, $k_p = 0$) and the controlled (right panels, $k_p = 0.05$) drifting oscillator under variation of excitation amplitude a calculated for $\alpha = 0.1$, $\beta = 0.1$, $\gamma = 1.0$, $\zeta = 0.05$, $g = 0.02$, $\omega = 0.53$, $\varphi = 0$, (a) $b = 0.1$, and (b) $b = 0.15$.

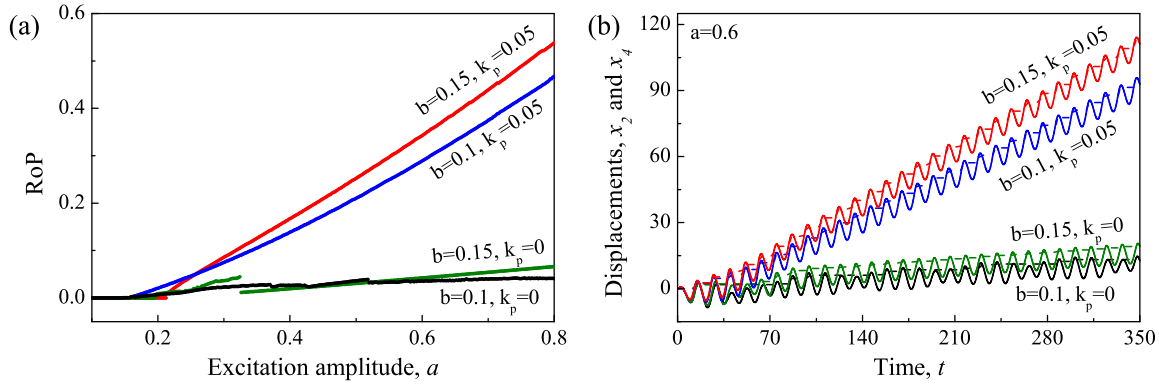

Figure 3.4: (Colour online) (a) ROPs for the uncontrolled and the controlled drifting oscillator under variation of excitation amplitude a calculated for $\alpha = 0.1$, $\beta = 0.1$, $\gamma = 1.0$, $\zeta = 0.05$, $g = 0.02$, $\omega = 0.53$, and $\varphi = 0$. (b) Displacements of the drill-bit (solid lines) and the slider bottom (dash lines) obtained for $\alpha = 0.1$, $\beta = 0.1$, $\gamma = 1.0$, $\zeta = 0.05$, $g = 0.02$, $\omega = 0.53$, $\varphi = 0$, and $a = 0.6$.

method which can maintain the best ROP at all the time accommodating/adjusting to the changes in the drilled formation. In this subsection, we will demonstrate the capability of the proposed position feedback controller for retaining the ROP of vibro-impact drilling under various rock formations. It should be noted that, according to the mathematical model of drifting oscillator used in this paper (see Fig. 2.1), the parameters β and γ were altered to reflect the change of hardness of rock formation, so the parameter ζ was affected accordingly. For example, if 20% softer formation is considered, the new parameters will be $\beta' = \frac{\beta}{0.8}$ and $\gamma' = \frac{\gamma}{0.8}$, and the corresponding damping ratio becomes $\zeta' = \zeta\sqrt{0.8} \approx 0.894\zeta$.

Fig. 3.6(a) presents the comparison between the ROPs obtained for the uncontrolled and the controlled

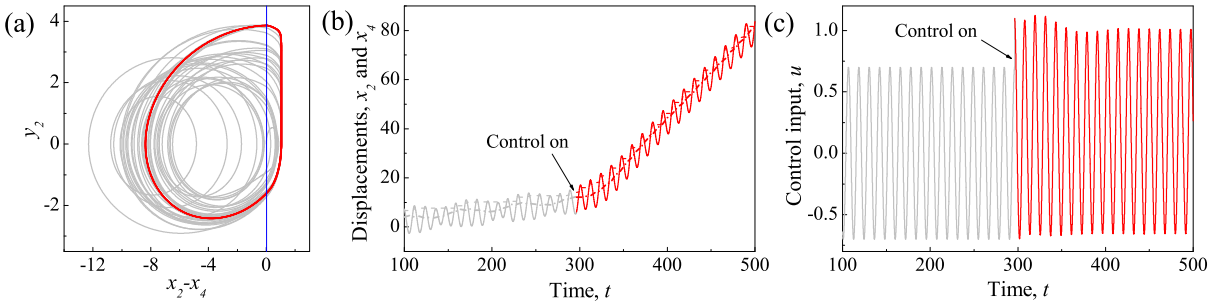

Figure 3.5: (Colour online) (a) Trajectory of the drifting oscillator on the phase plane (x_2-x_4, y_2), (b) time histories of displacements of the drill-string x_1 (dash-dot line), the drill-bit x_2 (solid line), and the slider bottom x_4 (dash line), and (c) time histories of the control input u before and after the application of the position feedback controller obtained for $\alpha = 0.1$, $\beta = 0.1$, $\gamma = 1.0$, $\zeta = 0.05$, $g = 0.02$, $\omega = 0.53$, $\varphi = 0$, $a = 0.7$, and $b = 0.1$. The position feedback controller ($k_p = 0.05$) was switched on from the 26^{th} period of external excitation, where $t \approx 296$. Grey and red lines represent the drifting oscillator before and after the application of the position feedback controller, respectively. The location of the impact surface, which indicates the contact of the drill-bit and the left plate of the frictional slider, is denoted by blue line on the phase plane.

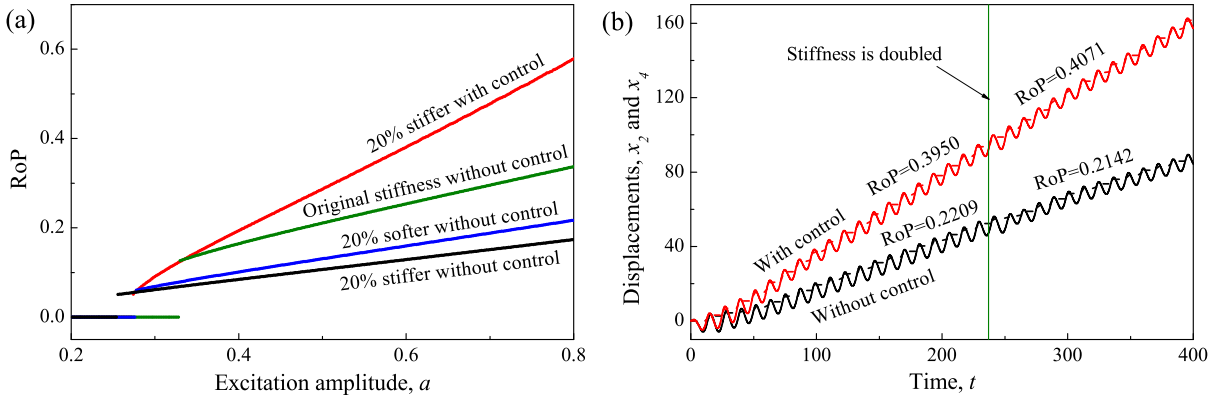

Figure 3.6: (Colour online) (a) ROPs for the uncontrolled and the controlled ($k_p = 0.05$) drifting oscillator under different rock mediums k_2 and variation of excitation amplitude a calculated for black: $\beta = 0.083$, $\gamma = 0.83$, $\zeta = 0.054$; blue: $\beta = 0.125$, $\gamma = 1.25$, $\zeta = 0.045$; green: $\beta = 0.1$, $\gamma = 1.0$, $\zeta = 0.05$; red: $\beta = 0.083$, $\gamma = 0.83$, $\zeta = 0.054$, $\alpha = 0.1$, $g = 0.02$, $\omega = 0.53$, $\varphi = 0$, and $b = 0.25$. (b) Time histories of displacements of the drill-bit x_2 (solid lines) and the slider bottom x_4 (dash lines) for the system with and without control obtained for $\alpha = 0.1$, $\beta = 0.1$, $\gamma = 1.0$, $\zeta = 0.05$, $g = 0.02$, $\omega = 0.53$, $\varphi = 0$, $a = 0.6$, $b = 0.25$, $k_p = 0$ (black lines), and $k_p = 0.05$ (red lines). At $t \approx 237.1$, the hardness of the drilled formation is doubled, so the new parameters become $\beta' = 0.05$, $\gamma' = 0.5$, $\zeta' = 0.07$.

drifting oscillator for various slider properties using the amplitude of excitation as a branching parameter. It can be clearly seen that, when the formation becomes 20% softer, the ROPs of drilling without control (blue dots) reduces comparing to the original drilled formation (green dots). Such decrease becomes worse when the drilled formation is 20% stiffer (black dots) than the original one. Once the control was applied, the ROPs for 20% stiffer formation was improved significantly. A further demonstration of efficiency of the proposed controller is displayed in Fig. 3.6(b), where displacements of the drill-bit and the slider bottom for the drifting oscillator with (red lines) and without control (black lines) are presented. As can be seen from the figure, the ROP of the drilling with control is 0.3950 and the one without control is 0.2209. When the hardness of the drilled formation is doubled at $t \approx 237.1$, the ROP with control increases to 0.4071, while the one without control decreases to 0.2142.

Bifurcation diagrams and ROPs as functions of excitation frequency ω of the uncontrolled drifting oscillator under various drilled formations are shown in Fig. 3.7. For the original drilled formation, the best ROP was recorded at $\omega = 0.428$. When the drilled formation becomes 20% softer, the best ROP was observed at $\omega = 0.47$. For both scenarios, it can be seen from Fig. 3.7(a) and (b) that, the frequencies for the best ROPs are very close to the regimes of chaotic motions. So, it is very likely that the vibro-impact

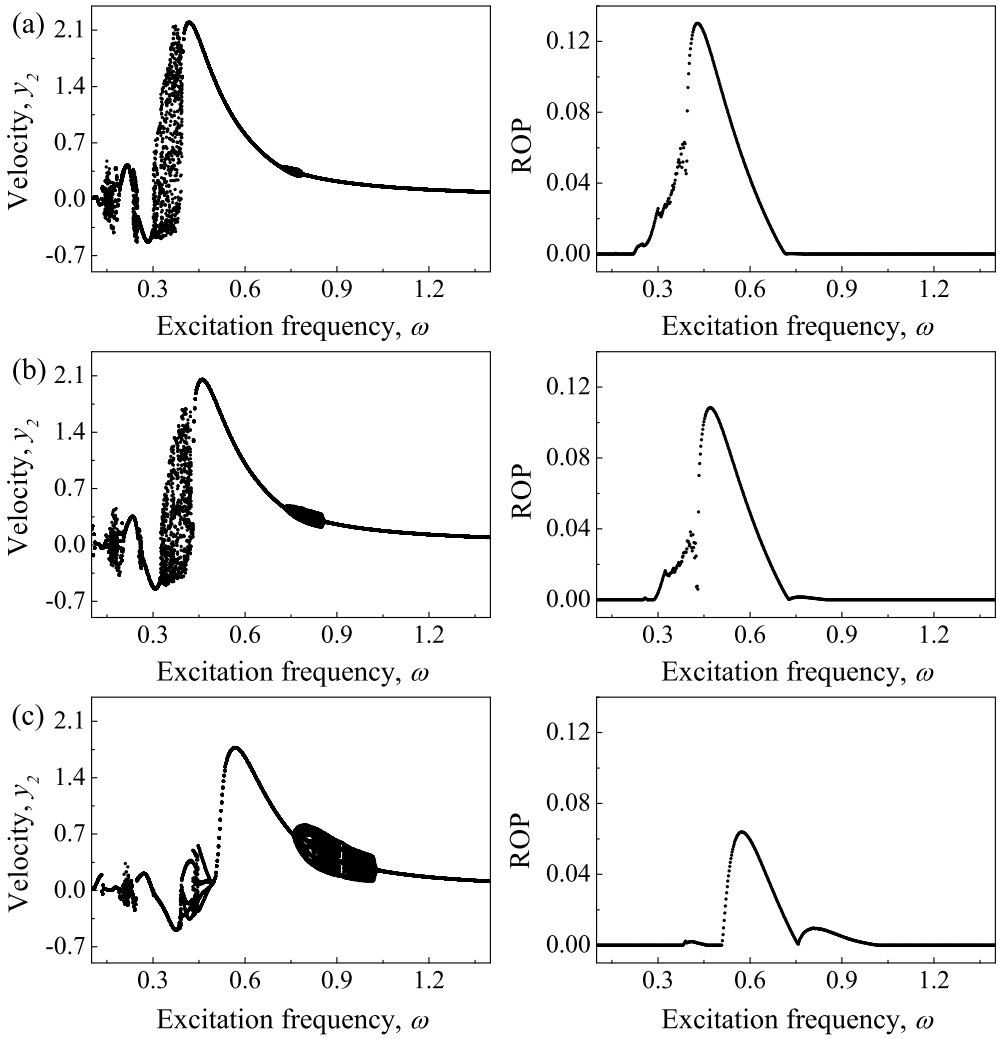

Figure 3.7: Bifurcation diagrams showing velocities (left panels) and ROPs (right panels) of the uncontrolled drifting oscillator under variation of excitation frequency ω calculated for $\alpha = 0.1$, $g = 0.02$, $\varphi = 0$, $a = 0.35$, $b = 0.2$ with (a) original stiffness: $\beta = 0.1$, $\gamma = 1.0$, $\zeta = 0.05$, (b) 20% softer: $\beta = 0.125$, $\gamma = 1.25$, $\zeta = 0.045$, and (c) 50% softer: $\beta = 0.2$, $\gamma = 2.0$, $\zeta = 0.0354$.

drilling is led to chaos due to perturbations or external disturbances when it is operated under the chosen excitation for the best ROP. When the drilled formation becomes 50% softer, such issue becomes better, i.e. the optimum frequency for the best ROP is far from the regime of chaotic motions, but the frequency range for periodic motion is still small.

Fig. 3.8 presents the bifurcation diagrams and ROPs of the controlled drifting oscillator ($k_p = 0.3$) under variation of excitation frequency ω. It can be seen that most of the chaotic motions have been suppressed, and the only chaotic regime recorded is $\omega \in (1.06, 1.158)$ for 50% softer drilled formation, where no penetration has been observed. Internal panels in these figures show the trajectories and displacements of the drilling at some frequencies presenting the best ROPs. The frequencies for the best ROPs of original, 20% softer, and 50% softer are recorded at $\omega = 0.820$, 0.844, and 0.898, respectively. It is interesting to see that, at low frequency $\omega \in (0.1152, 0.125)$, the controlled system has made some progressions. However, comparing the internal panels in Fig. 3.8(c), it is found that the drill-string m_1 (green line) has serious axial oscillations when the property of the slider is 50% softer, while the drill-string m_1 at other peak ROPs, e.g. $\omega = 0.820$, 0.844, and 0.898, has smooth progress with the drill-bit m_2. Thus, this oscillating regime which could cause drill-string instability should be avoided when the

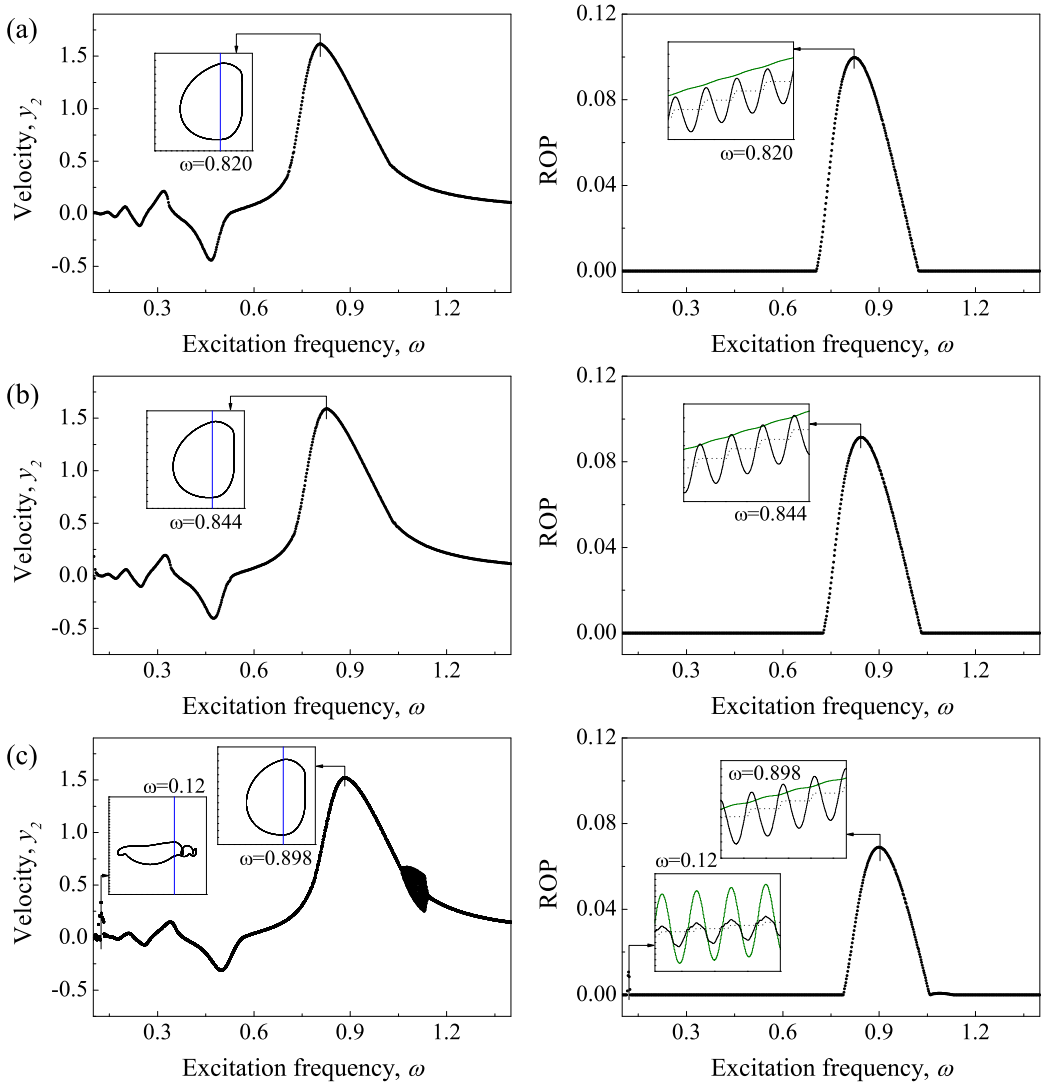

Figure 3.8: (Colour online) Bifurcation diagrams showing velocities (left panels) and ROPs (right panels) of the controlled ($k_p = 0.3$) higher order drifting oscillator under variation of excitation frequency ω calculated for $\alpha = 0.1$, $g = 0.02$, $\varphi = 0$, $a = 0.35$, $b = 0.2$ with (a) original stiffness: $\beta = 0.1$, $\gamma = 1.0$, $\zeta = 0.05$, (b) 20% softer: $\beta = 0.125$, $\gamma = 1.25$, $\zeta = 0.045$, and (c) 50% softer: $\beta = 0.2$, $\gamma = 2.0$, $\zeta = 0.0354$. Inner windows in the left panels present the trajectory of the oscillator on the phase plane (x_2-x_4, y_2), and the inner windows in the right panels show the time histories of displacements of the drifting oscillator. x_1, x_2, and x_4 are denoted by green, black solid, and black dash lines, respectively.

property of the slider becomes softer.

Fig. 3.9 analyzes the performance of the position feedback controller when the slider properties change. As can be seen from Fig. 3.9(a), the drifting oscillator is operated using the optimum frequency $\omega = 0.428$, without applying the position controller. When the slider becomes 50% softer, the motion of the drifting oscillator varies from period-one motion to aperiodic, and the progression rate drops drastically. When the controller is applied ($k_p = 0.3$) as shown in Fig. 3.9(b), although the ROP of the drifting oscillator reduces, the periodic motion of the drifting oscillator is not affected significantly. This also can be observed from the trajectories of the drill-string m_1 that, when the property of the slider varies, the uncontrolled drill-string fluctuates greatly, while the controlled drill-string behaves following a period-one response. The numerical observations reveal the effectiveness the position feedback controller from a practical point of view, since it allows the operator of a vibro-impact drilling rig to stabilize the system response to an operation mode with a meaningful ROP, even in the case when the properties of the drilled

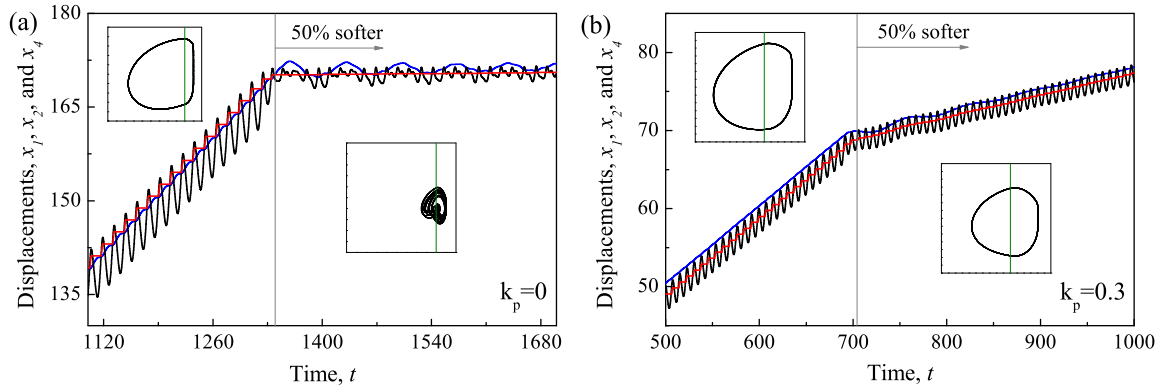

Figure 3.9: (Colour online) Time histories of displacements of m_1 (blue lines), m_2 (black lines), and the slider bottom (red lines) for the drifting oscillator (a) without control $k_p = 0$ at $\omega = 0.428$ and (b) with control $k_p = 0.3$ at $\omega = 0.82$ obtained for $\alpha = 0.1$, $g = 0.02$, $\varphi = 0$, $a = 0.35$, $b = 0.2$. The oscillator was operated under the original stiffness: $\beta = 0.1$, $\gamma = 1.0$, $\zeta = 0.05$, and after a number of periods of motion, the stiffness of the slider property becomes 50% softer: $\beta = 0.2$, $\gamma = 2.0$, $\zeta = 0.0354$. Inner windows present the trajectories of the oscillator before and after the stiffness of the slider property changes on the phase plane (x_2-x_4, y_2). The location of the impact surface, which indicates the contact of the drill-bit and the left plate of the frictional slider, is denoted by green line on the phase plane.

medium change, as shown in our numerical investigation.

4. Analysis of the system response via path-following methods

In this section we will present a detailed numerical investigation of the dynamical response of the vibro-impact drilling model given by Eq. (2.10). For this purpose, we will apply numerical continuation methods for non-smooth dynamical systems, implemented via the continuation platform COCO [32, 33]. Specifically, we will concentrate on the periodic response of the model observed in Fig. 3.1, which reveals the presence of coexisting attractors in the system. As could be seen in that figure, one attractor corresponds to a system behaviour for which the ROP is zero, while the other solution gives a nonzero ROP. In the present section we will determine whether the control method proposed in our study is able to eliminate this bistability, in such a way that an undesired transition from a progressing motion to an operation mode with zero ROP can be avoided.

4.1. One-parameter analysis

The starting point for our study via path-following methods is the periodic solution plotted in Fig. 3.1(d) (in black), corresponding to a system response with a positive ROP. In this case, the solution comprises the three operation modes described in the previous section: *no contact*, *contact without progression* and *contact with progression*. In Fig. 4.1(a) we present the result of the numerical continuation of this orbit with respect to the static force b. In this diagram, changes of stability are detected, which are marked with solid (for stable solutions) and dashed (unstable solutions) lines. As can be seen in the picture, for low values of b there is a branch of unstable periodic orbits with an ROP equal to zero, which means that the *contact with progression* mode is not present. If the parameter increases, a grazing bifurcation GR2 is detected for $b \approx 0.13554$, after which the ROP becomes positive, due to the birth of a solution segment corresponding to the *contact with progression* mode in the periodic orbit. Fig. 4.1(e) presents a blow-up of the bifurcation diagram near the bifurcation GR2. Here, it can be seen that for a somewhat larger value of the static force ($b \approx 0.13744$) a torus bifurcation TR is found. At this point, the periodic solution becomes stable, because a pair of complex-conjugate Floquet multipliers of the periodic solution crosses the unit circle from the outside, in such a way that all nontrivial multipliers of the periodic orbit have modulus less than one after TR.

In Fig. 4.1(f) a (stable) quasiperiodic solution is computed at the test point P5 ($b = 0.13720$), a system response that is produced by the torus bifurcation TR. From this point, a large segment of stable

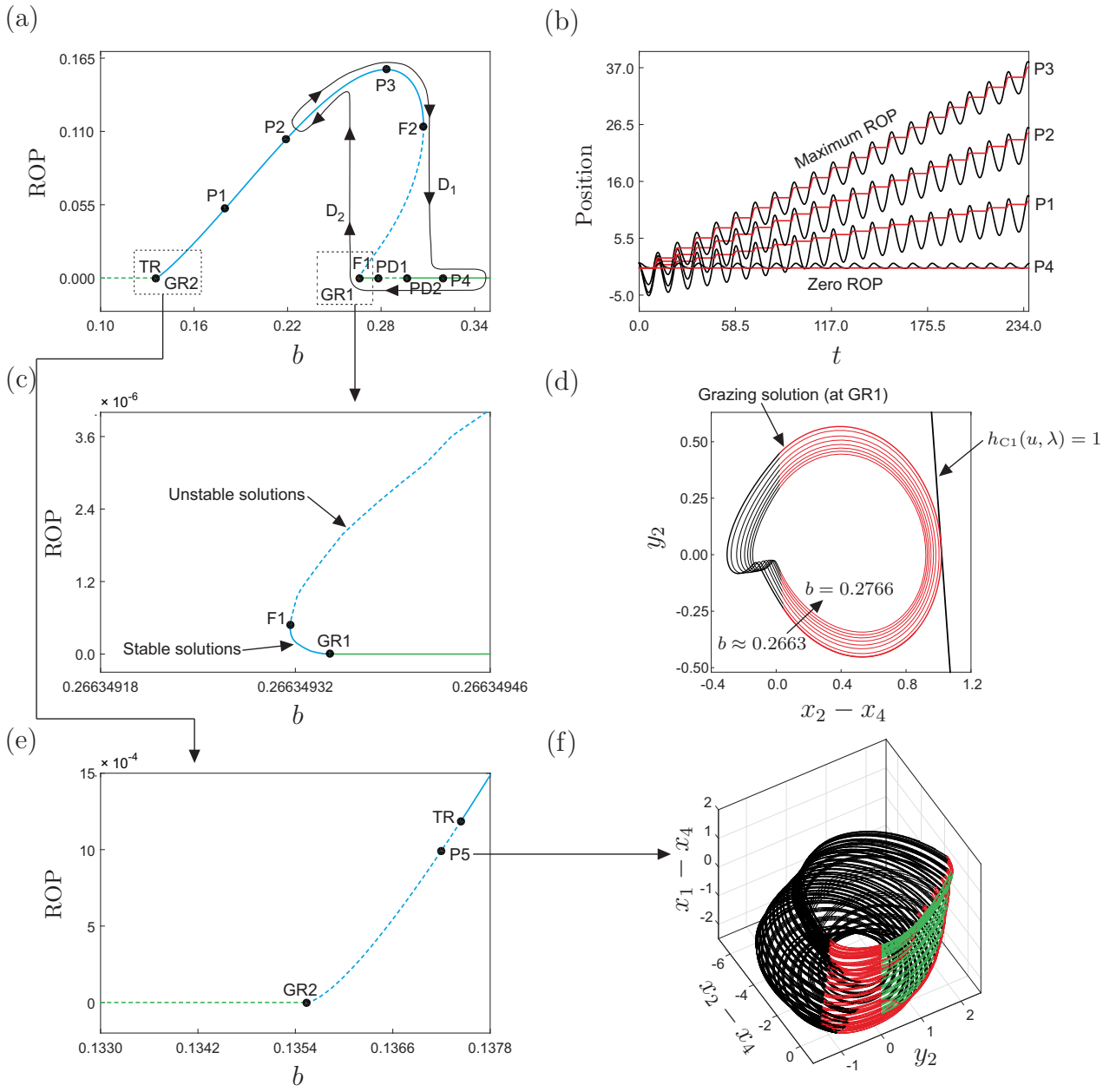

Figure 4.1: (a) Numerical continuation of the periodic orbit shown in Fig. 3.1(d) (in black) with respect to the static force b, computed for the parameter values $\alpha = 0.1$, $\beta = 0.1$, $\gamma = 1$, $\zeta = 0.05$, $a = 0.35$, $\omega = 0.53$, $\varphi = 0$, $g = 0.02$ and $k_p = 0$ (no control). The points TR, Fi GRi and PDi represent torus, fold, grazing and period-doubling bifurcations of limit cycles, while the labels Pi denote test points along the bifurcation diagram. The curve D_1–D_2 shows schematically a hysteresis loop of the system. (b) Time histories of the position of the mass m_2 (x_2, black) and the right plate of the frictional slider (x_4, red), computed at the test points Pi shown on panel (a). (c) Blow-up of the bifurcation diagram depicted in panel (a) around the grazing bifurcation GR1. (d) Family of periodic orbits computed near the grazing bifurcation GR1. The orbits are plotted with black and red colours that represent the modes *no contact* and *contact without progression*, respectively. The straight line stands for the discontinuity boundary $h_{C1}(u, \lambda) = 1$, which defines the transition from *contact without progression* to *contact with progression*. (e) Enlargement of the boxed region around the point GR2 shown in panel (a). (f) Quasiperiodic solution of the system near the torus bifurcation TR, computed at the test point P5. The black and red colours are as in panel (d). In addition, the green colour is used to mark the segments for which the system operates under the *contact with progression* mode.

periodic solutions is found, denoted by the solid blue curve in Fig. 4.1(a). This solid line finishes at $b \approx 0.30722$, where a fold bifurcation is found (F2). At this point, an unstable solution branch is born (dashed blue curve), which becomes solid again at another fold bifurcation labeled F1 ($b \approx 0.26634932$). Here, the periodic orbit becomes stable and after that undergoes a grazing bifurcation for $b \approx 0.26634934$. At this point, the mode *contact with progression* disappears from the periodic response, due to which the ROP becomes zero. The stable orbit with zero ROP persists for larger values of the static force b, until a period-doubling bifurcation PD1 is found at $b \approx 0.27833$. Here, a real Floquet multiplier leaves the unit circle through -1, due to which the (period-1) orbit loses stability and a stable period-2 solution is born. The unstable period-1 branch (dashed green line) finishes at $b \approx 0.29662$ (PD2), where another period-doubling bifurcation is detected. At this point, the real Floquet multiplier goes again inside the unit circle (through -1), and the stable period-2 solution disappears, while the period-1 orbit becomes stable and remains so for larger values of static force (within the parameter range considered in our computations).

Note that along the solid blue line shown in Fig. 4.1(a), a series of test points is computed, at the values $b = 0.18$ (P1), $b = 0.22$ (P2), $b \approx 0.28325$ (P3) and $b = 0.32$ (P4). The behaviour of the system at these points is presented in panel (b), which shows the time histories of the position of the mass m_2 (x_2) and the right plate of the frictional slider (x_4). As can be seen in the figure, the ROP varies from zero (at P4) to approximately 0.15642 (at P3), where the ROP achieves a maximum. On the other hand, a family of periodic orbits with zero ROP is plotted in Fig. 4.1(d), for the parameter range $0.2663 \leq b \leq 0.2766$. Note that during the contact modes it holds that $h_{\text{IMP}}(u, \lambda) = z_2 - z_3 - g = 0$ (see (2.10)), hence

$$\begin{aligned} h_{\text{C1}}(u, \lambda) &= 2\zeta w_2 + z_3 \\ &= 2\zeta w_2 + z_2 - g \\ &= 2\zeta y_2 + (x_2 - x_4) - g = 1, \end{aligned}$$

represents the discontinuity boundary (straight line in Fig. 4.1(d)) that defines the transition from *contact without progression* to *contact with progression*, as explained in Section 4. When a periodic orbit makes tangential contact with this boundary, a grazing bifurcation takes place, as shown in panel (d), corresponding to the grazing point GR1 displayed in panel (c).

Another important feature of the bifurcation scenario observed in the system is that there is a parameter window defined by the fold bifurcations F1 and F2 found before in which two attractors coexist (bistability). One attractor corresponds to a periodic solution with ROP positive, lying on the solid blue line plotted in Fig. 4.1(a). The other coexisting attractor is given by a system response with ROP zero. This second attractor, however, is divided into two types: one with period twice that of the external excitation (for b between the bifurcations PD1 and PD2) and one with the same period as the external excitation, obtained for b below PD1 and above PD2. The attractor on the solid blue line can be identified as a desirable solution from a practical point of view, since it yields an ROP positive. The other attractor, on the contrary, should be avoided, as it gives a zero progression that implies an inefficient use of energy. This motivates the study in the next section in which we will investigate whether the control scheme applied in this paper is able to eliminate the bistability.

4.2. Two-parameter analysis

Our numerical investigation so far has revealed the presence of various codimension-1 bifurcations that affect the behaviour of the system in different ways. In particular, the interplay between the fold bifurcations F1 and F2 gives rise to hysteresis in the system, which is schematically represented by the closed curve D_1–D_2 plotted in Fig. 4.1(a) and produced by the presence of two coexisting attractors for each b in a parameter window, as explained in the previous section. If, for instance, the system is set to yield the maximum ROP (found at the point P3 shown in Fig. 4.1(a)), an external perturbation may produce an undesired jump to the coexisting attractor with zero ROP, lying on the green branch depicted in the figure. One mechanism to deal with such a situation would be to use the hysteresis loop to switch back to the attractor with maximum ROP, which would require decreasing the static force below the fold point F1 so as to jump to the solid blue curve and then increasing the parameter until the optimal point P3 is reached again.

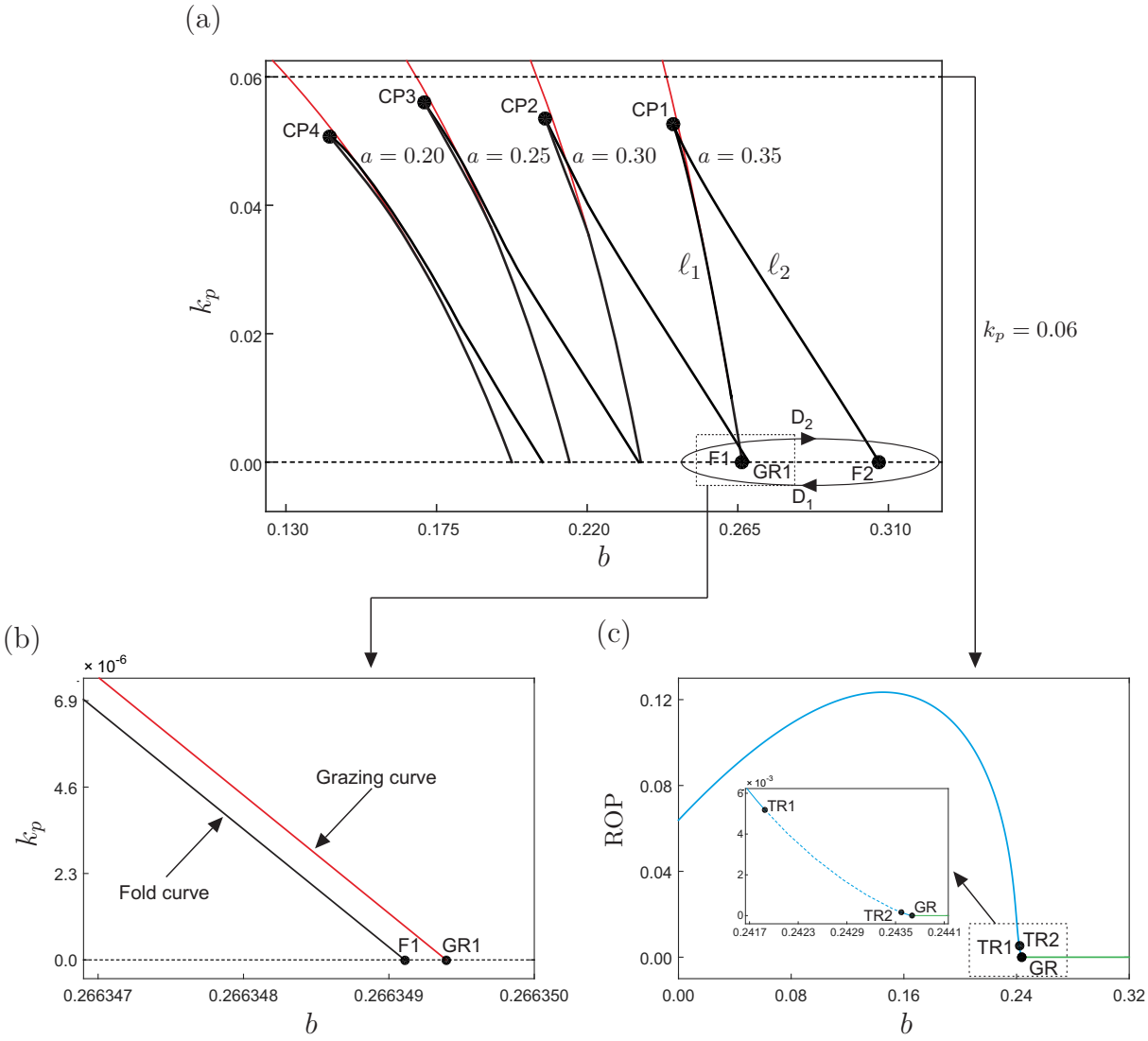

Figure 4.2: (a) Two-parameter continuation of the bifurcation points F1, F2 (both in black) and GR1 (red curve) shown in Fig. 4.1(a), with respect to the static force b and the control gain k_p. The resulting bifurcation diagram is computed for the cases $a = 0.35$, $a = 0.30$, $a = 0.25$ and $a = 0.20$. The curve D_1–D_2 shows schematically the hysteresis loop plotted in Fig. 4.1(a), obtained for $k_p = 0$ (no control). The points CPi denote a cusp bifurcation of limit cycles. (b) Blow-up of the bifurcation diagram in panel (a) around F1 and GR1. (c) One-parameter continuation with respect to the static force b. The parameter values are as in Fig. 4.1, except for $k_p = 0.06$. The inner panel depicts an enlargement of the boxed region.

In this section, we will investigate whether the control scheme applied to the vibro-impact drilling model can be used in order to eliminate the bistability, by suitably changing the control gain k_p. In order to gain an insight into this matter we will carry out a two-parameter continuation of the codimension-1 points F1, F2 and GR1, found in Fig. 4.1(a). These codimension-1 bifurcations play a fundamental role regarding the presence of bistability in the system, as will be seen in our numerical study. The result of the two-parameter continuation is presented in Fig. 4.2(a), for the cases $a = 0.35$, $a = 0.30$, $a = 0.25$ and $a = 0.20$. The labels F1, F2 and GR1 correspond precisely to the codimension-1 bifurcations detected in Fig. 4.1(a), for $a = 0.35$ and $k_p = 0$ (no control). Similarly, the curve D_1–D_2 shows schematically the hysteresis loop found before. The labels ℓ_1 and ℓ_2 denote the locus of fold points obtained from the two-parameter continuation of the bifurcations F1 and F2, respectively. The numerical computations reveal the presence of a codimension-2 point $(b, k_p) \approx (0.24561, 0.05269)$ (CP1), where the two fold branches, ℓ_1 and ℓ_2, join together via a cusp singularity. This dynamical phenomenon explains the presence of the

loop D_1–D_2 found in Fig. 4.1(a), as such hysteretic effects are known to occur near a cusp point (see [34, Section 8.2]). Further numerical computations indicate that the bifurcation scenario just explained is robust under small parameter variations, as its main qualitative features persists when the amplitude a is perturbed. In each case, a cusp singularity was found, for the values $(b, k_p) \approx (0.20927, 0.05391)$ (CP2), $(b, k_p) \approx (0.17331, 0.05603)$ (CP3) and $(b, k_p) \approx (0.14543, 0.05064)$ (CP4), when the amplitude of excitation is $a = 0.30$, 0.25, and 0.20, respectively.

Another remarkable feature of the bifurcation picture described above is the closeness between the fold branch ℓ_1 and the curve of grazing bifurcations plotted in red in Fig. 4.2(a). A closer look at this matter is given in panel (b), which shows a blow-up of the two-parameter bifurcation diagram near the points F1 and GR1. This is a dynamical scenario where a classical bifurcation (fold) is induced by a non-smooth bifurcation (grazing), which is a typical phenomenon observed in systems with soft impacts (cf. [35, 36] and [37, Example 2.3]). On the other hand, note that when k_p increases from zero the size of the interval of bistability, defined by the fold curves ℓ_1 and ℓ_2, decreases. A critical point is reached when the horizontal line $k_p = k_p^0$, $k_p^0 \geq 0$, reaches the cusp point CP1, above which the fold bifurcations defining the bistability disappear, see Fig. 4.2(a). Therefore, it can be seen that the control method applied to the vibro-impact drilling model is indeed capable of eliminating the bistability by suitably choosing the control gain k_p. Furthermore, this mechanism is robust under small parameter perturbations, as is confirmed by the series of bifurcation diagrams obtained for several values of amplitude a. An example of the effectiveness of this approach to eliminate bistability is presented in Fig. 4.2(c), where a one-parameter bifurcation diagram with respect to the static force b is computed for $k_p = 0.06$, above the cusp point CP1. Here, it can be seen that the hysteretic effects have been eliminated, and therefore the situation in which an undesired transition from an attractor with positive ROP to one with zero ROP is no longer possible, as it was in the case analyzed in Fig. 4.1(a), characterized by two coexisting attractors with positive and zero ROP, respectively.

5. Conclusions

This paper studied a position feedback control strategy for controlling a higher order drifting oscillator with application to the vibro-impact drilling. The cause of control issue for the drifting oscillator is twofold. Firstly, bistability has been observed when the drifting oscillator is operated in the optimum regime at where the main attractor generating the best ROP coexists with the attractor with no ROP. Secondly, the dynamics of the oscillator becomes chaotic when the static force (i.e. weight-on-bit) is applied insufficiently. In order to address these two issues, we proposed a position feedback controller which simply adopts the relative displacement between the mass m_2 and the right slider plate, and our studies mainly focused on exploring its capability in improving the ROP and suppressing bistability and chaos by using the path-following methods.

Our bifurcation analyses were carried out by using the static force, the frequency and the amplitude of excitation as branching parameters. For the scenario of using the static force as branching parameter, we have observed that the system is always bistable when the optimum static force, which produces the fastest ROP, is applied regardless of the amplitude of external excitation. This coexistence may cause the drilling inefficiency such that, the drilling system may experience the state hopping from the main attractor having the fastest ROP to the attractor with no ROP due to external perturbation. After applying the proposed controller, it has revealed that, the system was converted from bistable to monostable, and the attractor having no progression was successfully removed. From our calculations, we have found that, the ROP for the controlled drifting oscillator has been decreased, but as a compromise, the required static force providing the best ROP has been significantly reduced.

For the scenarios of using the frequency and the amplitude of external excitation, we have demonstrated the effectiveness of the proposed controller on suppressing chaos caused by insufficient static force. Some examples were given to show the controlled dynamics of the drill-bit for a wide frequency range of external excitation. In addition, we have studied the position feedback controller under varying drilled formations, since the optimum set of control parameters will be affected when the drilled formation is changed. From the study, we have found that, the ROP of uncontrolled drifting oscillator decreases when the drilled formation becomes either softer or stiffer. When the control was applied, under the condition

of varying drilled formation, the ROP of the system was significantly improved by appropriately choosing the feedback control gain.

To investigate the dynamical response of the drifting oscillator in detail, we have applied numerical continuation methods for non-smooth dynamics systems, implemented via the continuation platform COCO. Our concern has focused on whether we can eliminate the bistability in such a way that, an undesired transition from a progressing motion to a no progression one can be avoided. Based on our continuation studies, torus, grazing, fold, and period doubling bifurcations were identified in the drifting oscillator, which affect the behaviour of the system in different ways. From the one-parameter analysis, we have found a parameter window defined by the fold bifurcations $F1$ and $F2$ in which bistability was detected. Here, one attractor corresponds to a periodic solution with positive ROP, and the other coexisting attractor is given by a system response with zero ROP. The second attractor can be further divided into two types: one with period twice that of the external excitation and one with the same period as the external excitation.

For the two-parameter analysis, our studies have focused on the interplay between the fold bifurcations F1 and F2 giving rise to the hysteresis in the system. We have followed the codimension-1 points F1, F2, and GR1, which play a fundamental role regarding the presence of bistability in the system. Our numerical computations have revealed the presence of codimension-2 points, where the two fold branches join together via a cusp singularity. It has also indicated that the bifurcation scenario is robust under small parameter variations, as its main qualitative features persists when the amplitude of excitation is perturbed. Another remarkable finding of our two-parameter analysis is that, when the feedback control gain k_p increases, the size of the interval of bistability, defined by the fold curves decreases, and the bistability will disappear once the control gain reaches the cusp point. Therefore, this analysis allows us to identify the minimum control gain which guarantees eliminating the bistability.

Data accessibility statement. This work does not have any experimental data.

Competing interests statement. We have no competing interests.

Authors' contributions. YL carried out the brute force numerical study and led the writing of this manuscript; JPC carried out the numerical continuation and contributed to the writing of this manuscript partially; EP contributed to the modifications of the manuscript; MW provided recommendations to improve the manuscript. All authors gave final approval for submission.

Acknowledgements. The authors would like to thank all the three anonymous reviewers and the editor for their careful reading of the paper and valuable comments on the work.

Funding statement. This work was supported by the EPSRC grant EP/P023983/1.

Ethics statement. This work does not involve any ethical issue.

References

[1] G. R. Samuel, "Percussion drilling. is it a lost technique? a review.," in *SPE 35240, The Permian basin oil & gas recovery conference*, (Mildland, TX, USA), 1996.

[2] H. Rabia, "A unified prediction model for percussive and rotary drilling," *Mining Science and Technology*, vol. 2, no. 3, pp. 207–216, 1985.

[3] M. Wiercigroch, "Resonance enhanced drilling: method and apparatus," *Patent No. WO2007141550*, 2007.

[4] E. Pavlovskaia, M. Wiercigroch, and C. Grebogi, "Modeling of an impact system with a drift," *Phys. Rev. E*, vol. 64, p. 056224, 2001.

[5] E. Pavlovskaia and M. Wiercigroch, "Periodic solution finder for an impact oscillator with a drift," *J Sound Vib.*, vol. 267, pp. 893–911, 2003.

[6] G. W. Luo and X. H. Lv, "Dynamics of a plastic impact system with oscillatory and progressive motions," *Int. J. Nonlinear Mech.*, vol. 43, pp. 100–110, 2008.

[7] V. D. Nguyen, K. C. Woo, and E. Pavlovskaia, "Experimental study and mathematical modelling of a new of vibro-impact moling device," *Int. J. Nonlinear Mech.*, vol. 43, pp. 542–550, 2008.

[8] O. K. Ajibose, M. Wiercigroch, E. Pavlovskaia, and A. R. Akisanya, "Global and local dynamics of drifting oscillator for different contact force models," *Int. J. Nonlinear Mech.*, vol. 45, pp. 850–858, 2010.

[9] Q. Cao, M. Wiercigroch, E. Pavlovskaia, and S. Yang, "Bifurcations and the penetrating rate analysis of a model for percussive drilling," *Acta Mech. Sin.*, vol. 26, pp. 467–475, 2010.

[10] R. R. Aguiar and H. I. Weber, "Mathematical modeling and experimental investigation of an embedded vibro-impact system," *Nonlinear Dyn.*, vol. 65, pp. 317–334, 2011.

[11] E. Pavlovskaia and M. Wiercigroch, "Modelling of vibro-impact system driven by beat frequency," *Int. J. Mech. Sci.*, vol. 45, pp. 623–641, 2003.

[12] E. Pavlovskaia, D. Hendry, and M. Wiercigroch, "Modelling of high frequency vibro-impact drilling," *Int. J. Mech. Sci.*, vol. 91, pp. 110–119, 2015.

[13] G. L. Cavanough, M. Kochanek, J. B. Cunningham, and I. D. Gipps, "A self-optimizing control system for hard rock percussive drilling," *IEEE/ASME T. Mech.*, vol. 13, pp. 153–157, 2008.

[14] S. L. T. Souza and I. L. Caldas, "Controlling chaotic orbits in mechanical systems with impacts," *Chaos, Solitons and Fractals*, vol. 19, pp. 171–178, 2004.

[15] H. Dankowicz and J. Jerrelind, "Control of near-grazing dynamics in impact oscillators," *Proc. R. Soc. A*, vol. 461, pp. 3365–3380, 2005.

[16] S. L. T. de Souza, I. L. Caldas, and R. L. Viana, "Damping control law for a chaotic impact oscillator," *Chaos Soliton Fract.*, vol. 32, pp. 745–750, 2007.

[17] S. L. T. de Souza, I. L. Caldas, R. L. Viana, and J. M. Balthazar, "Control and chaos for vibro-impact and non-ideal oscillators," *Journal of Theoretical and Applied Mechanics*, vol. 46, pp. 641–664, 2008.

[18] G. W. Luo and X. H. Lv, "Controlling bifurcation and chaos of a plastic impact oscillator," *Nonlinear Analysis: Real World Applications*, vol. 10, pp. 2047–2061, 2009.

[19] J. Ing, E. Pavlovskaia, M. Wiercigroch, and S. Banerjee, "Experimental study of impact oscillator with one-sided elastic constraint," *Phil. Trans. R. Soc. A*, vol. 366, pp. 679–704, 2008.

[20] J. Ing, E. Pavlovskaia, M. Wiercigroch, and S. Banerjee, "Bifurcation analysis of an impact oscillator with a one-sided elastic constraint near grazing," *Physica D*, vol. 239, pp. 312–321, 2010.

[21] Y. Liu, M. Wiercigroch, J. Ing, and E. Pavlovskaia, "Intermittent control of co-existing attractors," *Phil. Trans. R. Soc. A*, vol. 371, p. 0120428, 2013.

[22] D. W. M. Veldman, R. H. B. Fey, and H. Zwart, "Impulsive steering between coexisting stable periodic solutions with an application to vibrating plates," *J. Comput. Nonlinear Dynam*, vol. 12, p. 011013, 2016.

[23] K. T. A. H. Hosseinloo, J. Slotine, "Robust and adaptive control of coexisting attractors in nonlinear vibratory energy harvesters," *J. Vib. Control*, vol. 0, p. 0, 2017.

[24] Y. Liu and J. Páez Chávez, "Controlling coexisting attractors of an impacting system via linear augmentation," *Physica D*, vol. 348, pp. 1–11, 2017.

[25] Y. Liu, E. Pavlovskaia, D. Hendry, and M. Wiercigroch, "Vibro-impact responses of capsule system with various friction models," *Int. J. Mech. Sci.*, vol. 72, pp. 39–54, 2013.

[26] Y. Liu, E. Pavlovskaia, M. Wiercigroch, and Z. K. Peng, "Forward and backward motion control of a vibro-impact capsule system," *Int. J. Nonlinear Mech.*, vol. 70, pp. 30–46, 2015.

[27] Y. Liu and J. Páez Chávez, "Controlling multistability in a vibro-impact capsule system," *Nonlinear Dyn.*, vol. 88, pp. 1289–1304, 2017.

[28] J. Páez Chávez, E. E. Pavlovskaia, and M. Wiercigroch, "Bifurcation analysis of a piecewise-linear impact oscillator with drift," *Nonlinear Dynamics*, vol. 77, no. 1-2, pp. 213–227, 2014.

[29] E. Pavlovskaia, M. Wiercigroch, K. C. Woo, and A. A. Rodger, "Modelling of ground moling dynamics by an impact oscillator with a frictional slider," *Meccanica*, vol. 38, pp. 85–97, 2003.

[30] E. Pavlovskaia and M. Wiercigroch, "Analytical drift reconstruction in visco-elastic impact oscillators," *Chaos, Solitons and Fractals*, vol. 19, pp. 151–161, 2004.

[31] M. Wiercigroch and Y. Liu, "Control method," *Patent No. US20160245064*, 2016.

[32] H. Dankowicz and F. Schilder, *Recipes for continuation*. Computational Science and Engineering, Philadelphia: SIAM, 2013.

[33] H. Dankowicz and F. Schilder, "An extended continuation problem for bifurcation analysis in the presence of constraints," *J. Comput. Nonlin. Dyn.*, vol. 6, no. 3, p. 031003, 2011. (8 pages).

[34] Y. A. Kuznetsov, *Elements of Applied Bifurcation Theory*, vol. 112 of *Applied Mathematical Sciences*. New York: Springer-Verlag, third ed., 2004.

[35] S. Banerjee, J. Ing, E. E. Pavlovskaia, M. Wiercigroch, and R. Reddy, "Invisible grazings and dangerous bifurcations in impacting systems: The problem of narrow-band chaos," *Physical Review E*, vol. 79, no. 3, 2009.

[36] J. Páez Chávez and M. Wiercigroch, "Bifurcation Analysis of Periodic Orbits of a Non-Smooth Jeffcott Rotor Model," *Commun. Nonlinear Sci. Numer. Simul.*, vol. 18, no. 9, pp. 2571–2580, 2013.

[37] M. di Bernardo, C. J. Budd, A. R. Champneys, P. Kowalczyk, A. Nordmark, G. Tost, and P. T. Piiroinen, "Bifurcations in nonsmooth dynamical systems," *SIAM Review*, vol. 50, no. 4, pp. 629–701, 2008.